Editors' Suggestion

Two-Dimensional Reconfigurable Non-Hermitian Gauged Laser Array

Zihe Gao,[1,*] Xingdu Qiao,[2,*] Mingsen Pan,[1,*] Shuang Wu,[1] Jieun Yim,[1] Kaiyuan Chen,[1] Bikashkali Midya,[3] Li Ge,[4,5] and Liang Feng[1,2,†]

[1]*Department of Materials Science and Engineering, University of Pennsylvania, Philadelphia, Pennsylvania 19104, USA*
[2]*Department of Electrical and Systems Engineering, University of Pennsylvania, Philadelphia, Pennsylvania 19104, USA*
[3]*Department of Physical Sciences, Indian Institute of Science Education and Research, Berhampur, Odisha 760003, India*
[4]*Department of Physics and Astronomy, College of Staten Island, CUNY, Staten Island, New York 10314, USA*
[5]*The Graduate Center, CUNY, New York, New York 10016, USA*

(Received 27 November 2022; accepted 11 May 2023; published 26 June 2023)

Topological effects in photonic non-Hermitian systems have recently led to extraordinary discoveries including nonreciprocal lasing, topological insulator lasers, and topological metamaterials, to mention a few. These effects, although realized in non-Hermitian systems, are all stemming from their Hermitian components. Here we experimentally demonstrate the topological skin effect and boundary sensitivity, induced by the imaginary gauge field in a two-dimensional laser array, which are fundamentally different from any Hermitian topological effects and intrinsic to open systems. By selectively and asymmetrically injecting gain into the system, we have synthesized an imaginary gauge field on chip, which can be flexibly reconfigured on demand. We show not only that the non-Hermitian topological features remain intact in a nonlinear nonequilibrium system, but also that they can be harnessed to enable persistent phase locking with intensity morphing. Our work lays the foundation for a dynamically reconfigurable on-chip coherent system with robust scalability, attractive for building high-brightness sources with arbitrary intensity profiles.

DOI: 10.1103/PhysRevLett.130.263801

Synchronization between lasers is of both fundamental and technological importance. When lasers, or more generally speaking, oscillators, are phase locked (i.e., synchronized), they oscillate at the same frequency, with well-defined phase relationships between them [1]. Phase locking between lasers promises quadratic power density enhancement, critical to many applications including free-space optical communications, light detection and ranging (LIDAR), see-through display, and laser additive manufacturing, to name a few. In many of these applications, dynamical reconfigurability of the beam pattern is highly desirable and can significantly enhance the system performance [2–5]. A robust phase locking mechanism, compatible with mode reconfigurability, would enable the next-generation arbitrarily shaped high-brightness sources, compatible with the increasing complexity in the system and algorithm developments and the demand of software-hardware codesign. However, existing mechanisms for phase locking and supermode selection require delicate configurations defined by photolithography, and the mode intensity profile cannot be dynamically controlled after fabrication.

In the past decade, non-Hermitian open systems have been extensively investigated with promising findings broadening both our physical understandings and next-generation functional device applications [6–16]. A distinct class of point-gapped topological non-Hermitian system, fundamentally different from any Hermitian topological systems, has been identified recently, and attracting great theoretical interest [17–21]. The imaginary gauge field, in particular, belongs to such class of non-Hermitian Hamiltonians not only unique to open systems, but also qualitatively different from other types of non-Hermiticity previously investigated in optics and lasers [13,22,23]. In addition to robustness against disorders, a hallmark of topological effects, a system with an imaginary gauge field also features the non-Hermitian skin effect, which is the accumulation of a macroscopic number of edge states at one of the open boundaries of the system, originating from its nonzero spectral winding number and closed-boundary versus open-boundary conditions correspondence. The topological nature of such effects promises directional anisotropic transport and phase locking with robustness against disorders and dynamical instabilities [24–27]. Experimentally, the non-Hermitian skin effect has been realized in a variety of classical and quantum synthetic materials, including one-dimensional (1D) photonic systems [28], two-dimensional electric circuits [29], active matter [30], and acoustic systems [31]. A reconfigurable imaginary gauge field has been demonstrated in 1D coupled lasers [32,33].

Inspired by the unique non-Hermitian topology of imaginary gauge fields [17–20], we experimentally report an on-chip phase locking mechanism that is compatible with mode morphing [34]. In a two-dimensional (2D) laser

array on a programmable active integrated platform on chip, by synthesizing the imaginary gauge field using unidirectional coupling, breaking reciprocity in each pseudospin, we harness the boundary dependence and topological nature of the non-Hermitian skin effect. For the first time, we implement a robust phase locking scheme that simultaneously enables mode reconfigurability, on-the-fly control of winding numbers, and the tunability of the gauge field strength. The imaginary-gauged coupling not only brings phase locking with scalability, robustness, and mode reconfigurability, but also provides additional gain integration into the system that enhances output power. With these simultaneous benefits, this coherent broad-area laser array platform represents a promising architecture for the pursuit of reconfigurable and high-brightness optical source [35,36]. The vast possibilities of reconfigurability in such a fully programmable anisotropically coupled array, together with its inherent nonlinearity in carrier dynamics, can be also explored for the study of exotic physics and dynamics in non-Hermitian topology in point-gapped systems [18,21,37].

Our work demonstrates that the topological skin effect remains intact in a nonlinear laser system, and it can be harnessed to enable a robust phase-locked broad-area laser array compatible with dynamic mode reshaping.

We consider a non-Hermitian gauged laser array consisting of microring lasers on a square lattice. To introduce asymmetric coupling between nearest-neighbor microring cavities, we connect them with spiral-shaped coupling arms [see Fig. 1(a)]. Each microring cavity supports two degenerate lasing modes with the same whispering gallery mode (WGM) order but opposite power flow directions, one in the clockwise (CW) direction and the other in the counterclockwise (CCW) direction. We will refer to them conveniently as two pseudospins, and the coupling arms introduce nearest-neighbor hopping between modes with the same pseudospin. With asymmetric pumping on the coupling arms, we break the reciprocity in coupling for each pseudospin, creating an ultrafast-controllable non-Hermitian gauge field [32,33,38]. For example, for the CW

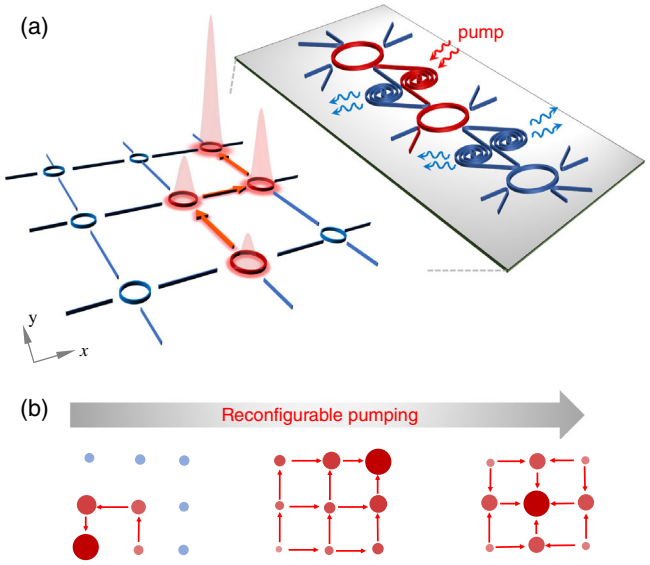

FIG. 1. The non-Hermitian gauged laser array with reconfigurable unidirectional coupling and skin effect coherent modes: (a) The reconfigurable coupling architecture implemented in spiral-shaped coupling arms. With amplification in one direction (red) and dissipation in the other direction (blue), unidirectional coupling (red arrows) is implemented, phase locking all lasers in the path with a skin effect optical mode. (b) Reconfigurable skin effect modes controlled by dynamic shaping of pumping profile.

pseudospin in Fig. 1(a), the photons hopping along the direction of the red arrows are amplified, while photons hopping against the direction of the red arrows undergo dissipation. The amplification or dissipation in each spiral arm is individually controlled using a spatial light modulator (SLM) that shapes the spatial profile of the optical pump beam [39].

The asymmetric coupling for the CCW pseudospin can be described by the following generalized Hatano-Nelson model [45]:

$$H_{2D,\circlearrowleft} = -\sum_{m,n} e^{h_R+i\phi_R} a^{\dagger}_{m+1,n,\circlearrowleft} a_{m,n,\circlearrowleft} + e^{h_L+i\phi_L} a^{\dagger}_{m,n,\circlearrowleft} a_{m+1,n,\circlearrowleft} + e^{h_U+i\phi_U} a^{\dagger}_{m+1,n,\circlearrowleft} a_{m,n,\circlearrowleft} + e^{h_D+i\phi_D} a^{\dagger}_{m,n,\circlearrowleft} a_{m+1,n,\circlearrowleft}, \quad (1)$$

where $\{a^{\dagger}_{m,n,\circlearrowleft}, a_{m,n,\circlearrowleft}\}$ are the 2D boson creation and annihilation operators for the CCW pseudospin at lattice coordinates (m,n), $h_{L,R} \in R$ ($h_{U,D} \in R$) are the imaginary gauge field strengths for coupling in positive and negative directions in x (y), leading to anisotropic couplings in the 2D plane, and $\phi_{R,L,U,D}$ represents real gauge fields. The two pseudospins in our system are connected by time-reversal symmetry, and hence the CW pseudospin experiences opposite gauge fields [39] by exchanging left and right, as well as up and down, in Eq. (1). Experimentally, the two pseudospins can be imaged separately as they emit orthogonal circular polarizations [46].

A 2×2 reconfigurable non-Hermitian gauged laser array is shown in Fig. 2(a). The four microring lasers are designed with an inner radius of 3 μm and a width of 600 nm. To extract light from the WGM inside the microring cavity, periodic scatters are inscribed along the inner sidewall of the microring [46]. The spiral coupling arm is optimized to ensure sufficient amplification or dissipation with a compact footprint: While the density of the spiral (distance between adjacent loops) is chosen to maximize the available gain without introducing back coupling, the central s bend is optimized to minimize the bending loss [47]. Theoretically, it can be shown that by

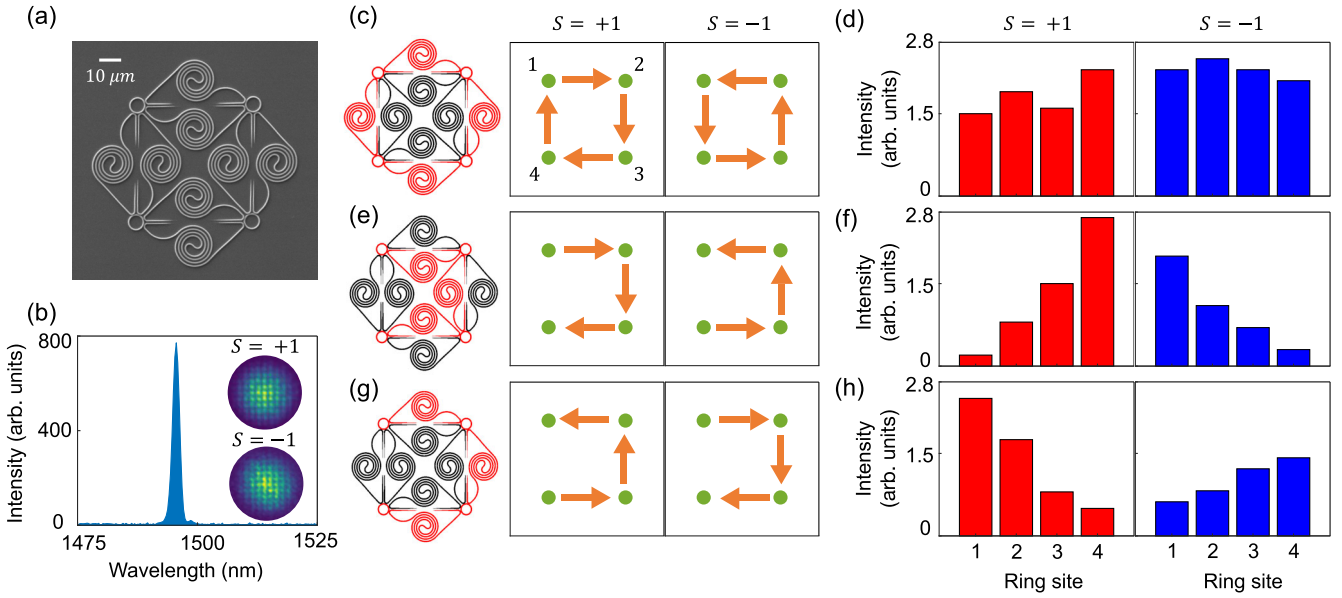

FIG. 2. A reconfigurable 2×2 non-Hermitian gauged laser array: (a) The scanning electron microscope (SEM) image of the array, fabricated on 200-nm-thick InGaAsP multiple quantum wells. (b) An example spectrum and far-field interference pattern (inset), showing the single-mode operation (phase locking) measured from both the CW and CCW pseudospins. The two pseudospins generate emissions in orthogonal circular polarizations (labeled by $S = \pm 1$, respectively) and are separately imaged. More interference images demonstrating phase locking for each configuration are shown in the Supplemental Material [39]. (c) and (d) Periodic boundary configuration, with pumped waveguides shown in red and unpumped in black. The intensity distribution is approximately equal in all lasers for each pseudospin. (e) and (f) Open boundary configuration demonstrating non-Hermitian skin effect, with intensity concentrating on boundaries of the array (opposite boundaries for the two pseudospins). (g) and (h) Open boundary configuration with opposite coupling direction compared to (e) and (f). Although the relative phase between the lasers were not intentionally controlled, the maximum intensity in the far field shown in the inset of (b) is ~2 times stronger than the incoherent summation of individual laser intensities.

connecting lasers with unidirectional coupling, we can make a single-supermode phase-locked array with gain suppression (between the lasing mode and the second-highest-gain mode) that is proportional to the coupling strength (see Supplemental Material [39]) [25,26,35]. This gain suppression can be explained as follows: For a weak imaginary gauge field or even in the absence of this gauge field, the intensity patterns of the lowest threshold supermodes are different. Therefore, after the first mode has turned on, the other modes can utilize the gain at places where the first mode has a weak intensity. However, with a strong imaginary gauge field, their intensities are all similar due to the topological nature of the non-Hermitian skin effect and all the supermodes compete for the same gain where they are localized. Once the first mode is above threshold, it strongly clamps the gain at that position and hence makes other modes difficult to reach their thresholds.

Experimentally, we show phase-locked single-mode lasing in three example configurations [Figs. 2(c)–2(h)]. With the freedom in choosing the direction of coupling or no coupling at all between each pair of nearest neighbors in the 2×2 array, these three configurations demonstrate boundary dependence, a signature of the non-Hermitian skin effect, and mode reconfigurability compatible with single mode lasing. When the asymmetric coupling forms a loop, the array is a 1D chain with periodic boundary condition, and for each pseudospin, the intensity distribution is balanced between all rings [Figs. 2(c) and 2(d)]. When we break the loop, the array experiences open boundary condition, and the non-Hermitian skin effect can be observed, where the intensity is concentrated on the edges [Figs. 2(e)–2(h)], while all the lasers are still phase locked. This strong boundary dependence is a key signature of the skin effect originating from non-Hermitian topology [18,25]. Single-mode operation (i.e., stable phase locking) is confirmed by interference fringes in the far field in all cases [shown in the inset of Fig. 2(b) and Supplemental Material [39]]. The 1D chain with periodic boundary condition in Fig. 2(c) can be characterized by a $w = \pm 1$ winding number for CCW and CW pseudospins, respectively, with w defined in an infinite (bulk) 1D system by $w = \int_0^{2\pi} (dk/2\pi i) \partial_k \ln E(k)$, where $E(k)$ is the momentum-dependent complex-valued energy in the first Brillouin zone [18]. The two open-boundary scenarios, shown in Figs. 2(e) and 2(g), respectively, are effectively 1D chains with opposite signs of winding numbers [39]. Winding number of $w > 0$ leads to localization at the right boundary, while winding number of $w < 0$ leads to localization at the left. Note that the winding numbers here are topological invariants, independent of the actual amplitude or phase of

the coupling coefficient t. Without disorders or nonlinearity, the unidirectional coupling results in a high-order EP and complete power concentration on the laser element on the boundary [39]. However, magnetic disorder and nonlinearity spoil this high-order EP and create finite tail in the localized intensity distribution that we experimentally observe. This intensity distribution is modeled with a set of rate equations that takes into account both photon and carrier dynamics, described in Supplemental Material, Sec. 3 [39].

With unidirectional coupling, we directly phase lock a 3×3 laser array, with $\sim$1.5 nm random detuning (nonmagnetic disorder) between laser elements, without any additional supermode selection mechanism, as shown in Fig. 3. The advantage of unidirectional coupling is also indicated by comparing to a symmetrically coupled array. In the same array, if we switch asymmetric coupling to symmetric, the array loses phase locking and becomes multimode (see Supplemental Material, Figs. S19 and S22 [39]). When the imaginary gauge field is uniform with unidirectional coupling in both the x and y directions, the non-Hermitian skin effect manifests as corner modes [Figs. 3(b) and 3(c)] [48,49], which are confined in both x and y dimensions. This 2D square lattice under a uniform imaginary gauge field is separable in the x and y dimensions, and the Hamiltonian can be written as a Kronecker sum of 1D Hamiltonians $H_{2D} = H_x \oplus H_y$. With this separability in our system, we can use a pair of 1D winding numbers, $\boldsymbol{w} = (w_x, w_y)$ in our 2D system. In Figs. 3(b) and 3(c), this winding number pair is $\boldsymbol{w} = (-1, -1)$ and (1,1), respectively, for the CCW pseudospin. We note that these 1D winding numbers in the 2D system are weak topological

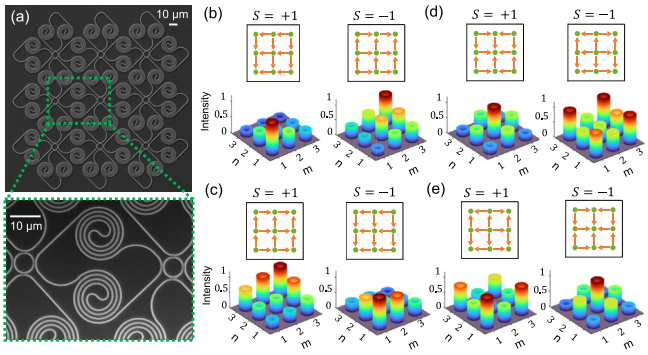

FIG. 3. A reconfigurable 3×3 non-Hermitian gauged laser array. (a) SEM images. (b) and (c) Non-Hermitian skin effect in two dimensions, with uniform winding numbers, $\boldsymbol{w} = (\mp 1, \mp 1)$ for the two pseudospins in (b) and $\boldsymbol{w} = (\pm 1, \pm 1)$ in (c). Directions of the coupling are shown in the upper panels and intensity distributions are shown in the lower panels, for the two pseudospins, respectively, separately imaged with opposite circular polarizations ($S = \pm 1$). (d) and (e) Non-Hermitian skin effects with corner modes at artificial domain boundaries, formed by nonuniform imaginary gauge field with different winding number pairs in each quadrant.

invariants and different from the strong topological invariants unique to high-dimensional systems [50–52]. When the imaginary gauge field changes direction within the 2D lattice, the non-Hermitian skin effect manifests as interface modes localized at the domain boundaries. For example, a mode localized at the center of the array can be configured with a judicious choice of coupling directions, with $\boldsymbol{w} = (-1, -1)$, $(1, -1)$, $(1,1)$, $(-1, 1)$ in the top right, top left, bottom left, and bottom right four quadrants [Figs. 3(d) and 3(e)]. Reversing the gauge field in each quadrant causes the mode to be localized equally in the four corners. This nonuniform anisotropic coupling offers vast possibilities of mode reconfigurability, which is different from another mechanism by changing the pump patterns on the microcavities themselves [53]. With a binary choice of coupling direction between each pair of neighboring lasers, there are 2^{12} configurations in this 3×3 array.

In addition to the binary control, we demonstrate the fine-tuning of array intensity distribution with coupling strength. The degree of localization in the optical mode increases with amplification in the coupling arms [Figs. 4(a) and 4(b)]. Moreover, the amplification from the imaginary-gauged coupling also contributes to the increase of total output power. In other words, the amplification in the coupling arms not only introduces an imaginary gauge field that creates phase locking but also contributes to increased output power beyond the simple summation of uncoupled rings, shown in Fig. 4(c).

Although the skin effect and corner modes can be qualitatively explained by the free-boson linear Hamiltonians in Eq. (1), the quantitative intensity distribution in our unidirectionally coupled laser array and the change of it according to the coupling strength [Figs. 4(a) and 4(b)] can only be explained with a nonlinear model that includes both carrier and photon dynamics in the laser cavities. While the photon evolution is governed by Eq. (1) or in the presence of disorders by the Hamiltonian in Supplemental Material, Sec. 2 [39], the carrier density in each laser cavity can dynamically modify the onsite gain and loss rate and the resonant frequency (through the Henry linewidth enhancement factor α_H). On the other hand, the local photon density determines the carrier depletion rate in each cavity (i.e., spatial hole burning). These nonlinear effects are most evidently illustrated in Figs. 4(a) and 4(b), where the total intensity distribution (summation of both pseudospins) remains approximately constant across the array albeit the significant changes in the intensity distributions for each spin caused by the imaginary gauge field. This invariance of summed intensity distribution is directly contrary to the linear model and can only be explained by the nonlinear dynamics [39]. By numerical integration of the nonlinear rate equations, we show steady-state solutions in Figs. 4(d) and 4(e). Temporal dynamics show that these steady states are stable phase-locked states [39]. The nonlinear effects, especially when the coupling

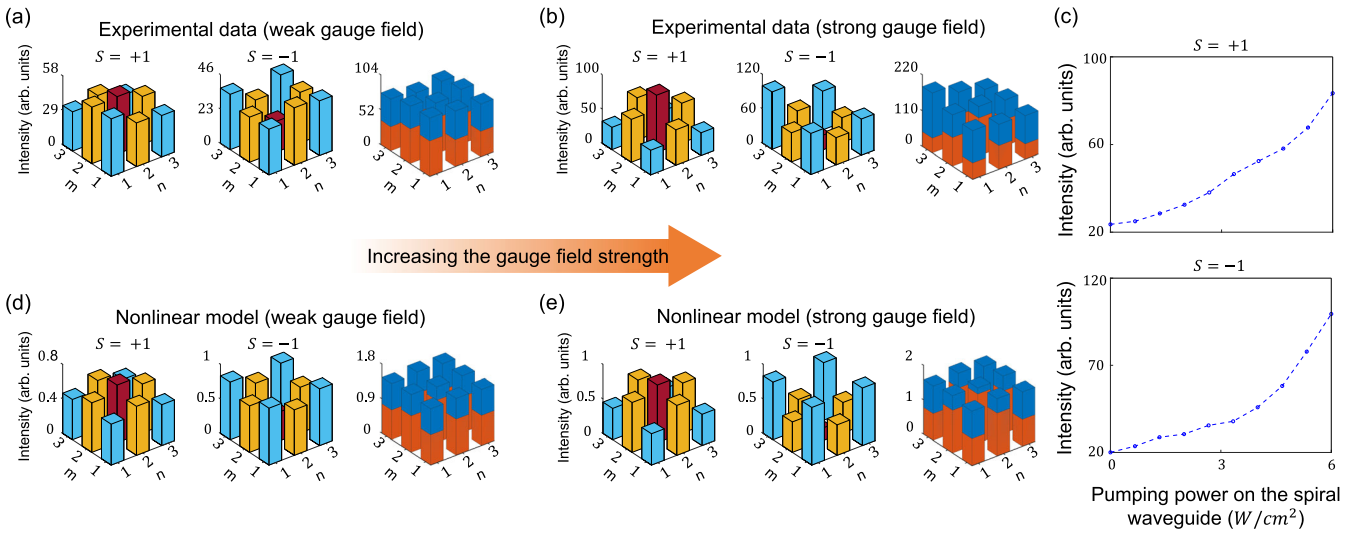

FIG. 4. The skin effect array under increasing coupling strength: (a) and (b) Experimental measurements of the intensity distributions under two different coupling strengths, while the pumping on microrings stay unchanged. The intensities in each pseudospin (labeled by $S = \pm 1$) and the total intensity (summation of $S = 1$ and $S = -1$) are shown. (c) Array output power in each pseudospin with increasing coupling strength (i.e., increasing optical pumping levels on the spiral waveguides, while the pumping levels on the laser cavities are unchanged). (d) and (e) Intensity distributions calculated from the nonlinear model, under two different coupling strengths [13 GHz for weak gauge field in (d) and 26 GHz for strong gauge field in (e)].

coefficients are weaker than or comparable to the inverse of photon lifetime, tend to balance the photon density distribution according to the pump profile, through spatial hole burning [40,41]. The nonlinear model we show here, calculated numerically with 45 rate equations for 9 lasers, are readily scalable to larger-scale laser arrays, and can guide future studies of more sophisticated temporal dynamics in such systems for modulation speed enhancement [54,55], photonic optimization [56], and neuromorphic computing [57].

In summary, we have demonstrated the first 2D non-Hermitian gauged laser array with on-chip reconfigurable asymmetric coupling, a promising platform for robust phase locking and mode reshaping. When configured to realize an effective 1D chain with either periodic or open boundary conditions, we demonstrate boundary condition dependent laser emission, a hallmark of non-Hermitian skin effect. With 2D configurations, we demonstrate reconfigurable corner modes, localized at the corners, or inside the bulk by artificially creating topological domain walls. The demonstrated unidirectional coupling assisted non-Hermitian gauge field promises robustness against disorders and compatibility with mode morphing, as a result of the topological nature of the non-Hermitian skin effect, desirable for the ever-going demand of scaling and reconfigurability in photonic circuits. One of the unique abilities of our devices is the external control of coupling enhancement between lasers. This provides an additional increase in output power, making the device attractive as future high-brightness sources. At last, we show the effect of nonlinearity and carrier dynamics in our array, providing guidance for future endeavors to harness dynamical effects, including modulation speed enhancement and photonic computing. The phase synchronization and the mutual coherence between lasers reported here lay the foundation for the demonstration of coherent combining and quadratic power density enhancement in the non-Hermitian gauged laser arrays in the future.

We acknowledge the support from Army Research Office (ARO) (W911NF-21-1-0148) and National Science Foundation (NSF) (ECCS-1846766, ECCS-1932803, and PHY-1847240). This work was partially supported by NSF through the University of Pennsylvania Materials Research Science and Engineering Center (MRSEC) (DMR-1720530) and carried out in part at the Singh Center for Nanotechnology, which is supported by the NSF National Nanotechnology Coordinated Infrastructure Program under Grant No. NNCI-1542153.

*These authors contributed equally to this work.
†fenglia@seas.upenn.edu

[1] H. G. Winful and S. S. Wang, Appl. Phys. Lett. **53**, 1894 (1988).
[2] J. Guehring, in *Videometrics and Optical Methods for 3D Shape Measurement* (SPIE, Bellingham, 2000), Vol. 4309, pp. 220–231, 10.1117/12.410877.
[3] M. Young, E. Beeson, J. Davis, S. Rusinkiewicz, and R. Ramamoorthi, in *Proceedings of the 2007 IEEE Conference on Computer Vision and Pattern Recognition* (IEEE, New York, 2007), pp. 1–8, 10.1109/CVPR.2007.383292.

[4] G. Wetzstein, D. Lanman, D. Gutierrez, and M. Hirsch, in *ACM SIGGRAPH 2012 Courses* (Association for Computing Machinery, New York, NY, USA, 2012), pp. 1–159, 10.1145/2343483.2343487.

[5] A. H. Dorrah and F. Capasso, in *Plasmonics: Design, Materials, Fabrication, Characterization, and Applications XX* (SPIE, Bellingham, 2022), Vol. PC12197, p. PC1219707, 10.1117/12.2634175.

[6] C. E. Rüter, K. G. Makris, R. El-Ganainy, D. N. Christodoulides, M. Segev, and D. Kip, Nat. Phys. **6**, 192 (2010).

[7] S. Longhi, Phys. Rev. A **82**, 031801(R) (2010).

[8] L. Chang, X. Jiang, S. Hua, C. Yang, J. Wen, and L. Jiang, Nature (London) **8**, 524 (2014).

[9] T. E. Lee and C.-K. Chan, Phys. Rev. X **4**, 041001 (2014).

[10] L. Feng, R. El-Ganainy, and L. Ge, Nat. Photonics **11**, 752 (2017).

[11] H.-K. Lau and A. A. Clerk, Nat. Commun. **9**, 4320 (2018).

[12] B. Midya, H. Zhao, and L. Feng, Nat. Commun. **9**, 2674 (2018).

[13] H. Zhao, X. Qiao, T. Wu, B. Midya, S. Longhi, and L. Feng, Science **365**, 1163 (2019).

[14] Y. Wu, W. Liu, J. Geng, X. Song, X. Ye, C.-K. Duan, X. Rong, and J. Du, Science **364**, 878 (2019).

[15] Ş. K. Özdemir, S. Rotter, F. Nori, and L. Yang, Nat. Mater. **18**, 783 (2019).

[16] Y. Li, Y. G. Peng, L. Han, M. A. Miri, W. Li, M. Xiao, and X. F. Zhu, Science **364**, 170 (2019).

[17] S. Yao and Z. Wang, Phys. Rev. Lett. **121**, 086803 (2018).

[18] N. Okuma, K. Kawabata, K. Shiozaki, and M. Sato, Phys. Rev. Lett. **124**, 086801 (2020).

[19] K. Zhang, Z. Yang, and C. Fang, Phys. Rev. Lett. **125**, 126402 (2020).

[20] D. S. Borgnia, A. J. Kruchkov, and R.-J. Slager, Phys. Rev. Lett. **124**, 056802 (2020).

[21] J. Claes and T. L. Hughes, Phys. Rev. B **103**, L140201 (2021).

[22] L. Feng, Z. J. Wong, R.-M. Ma, Y. Wang, and X. Zhang, Science **346**, 972 (2014).

[23] H. Hodaei, M.-A. Miri, M. Heinrich, D. N. Christodoulides, and M. Khajavikhan, Science **346**, 975 (2014).

[24] S. Longhi, D. Gatti, and G. Della Valle, Sci. Rep. **5**, 13376 (2015).

[25] S. Longhi, Opt. Lett. **47**, 2040 (2022).

[26] B. Zhu, Q. Wang, D. Leykam, H. Xue, Q. J. Wang, and Y. D. Chong, Phys. Rev. Lett. **129**, 013903 (2022).

[27] B. Midya, Phys. Rev. A **106**, 053513 (2022).

[28] S. Weidemann, M. Kremer, T. Helbig, T. Hofmann, A. Stegmaier, M. Greiter, R. Thomale, and A. Szameit, Science **368**, 311 (2020).

[29] T. Hofmann, T. Helbig, F. Schindler, N. Salgo, M. Brzezińska, M. Greiter, T. Kiessling, D. Wolf, A. Vollhardt, A. Kabaši, C. H. Lee, A. Bilušić, R. Thomale, and T. Neupert, Phys. Rev. Res. **2**, 023265 (2020).

[30] L. S. Palacios, S. Tchoumakov, M. Guix, I. Pagonabarraga, S. Sánchez, and A. G Grushin, Nat. Commun. **12**, 4691 (2021).

[31] X. Zhang, Y. Tian, J.-H. Jiang, M.-H. Lu, and Y.-F. Chen, Nat. Commun. **12**, 5377 (2021).

[32] Z. Zhang, X. Qiao, B. Midya, K. Liu, J. Sun, T. Wu, W. Liu, R. Agarwal, J. M. Jornet, S. Longhi, N. M. Litchinitser, and L. Feng, Science **368**, 760 (2020).

[33] Z. Zhang, H. Zhao, S. Wu, T. Wu, X. Qiao, Z. Gao, R. Agarwal, S. Longhi, N. M. Litchinitser, L. Ge, and L. Feng, Nature (London) **612**, 246 (2022).

[34] W. Wang, X. Wang, and G. Ma, Nature (London) **608**, 50 (2022).

[35] S. Longhi and L. Feng, APL Photonics **3**, 060802 (2018).

[36] S. Jiang, S. S. Deka, S. H. Pan, and Y. Fainman, IEEE J. Sel. Top. Quantum Electron. **28**, 1800312 (2022).

[37] K. Kawabata, K. Shiozaki, M. Ueda, and M. Sato, Phys. Rev. X **9**, 041015 (2019).

[38] Z. Zhang, H. Zhao, D. G. Pires, X. Qiao, Z. Gao, J. M. Jornet, S. Longhi, N. M. Litchinitser, and L. Feng, Light Sci. Appl. **9**, 179 (2020).

[39] See Supplemental Material at http://link.aps.org/supplemental/10.1103/PhysRevLett.130.263801 for theory, fabrication, and characterization details, which includes Refs. [1,25,32,40–44].

[40] L. Ge, Y. D. Chong, and A. D. Stone, Phys. Rev. A **82**, 063824 (2010).

[41] Z. Gao, M. T. Johnson, and K. D. Choquette, J. Appl. Phys. **123**, 173102 (2018).

[42] M. J. Adams, N. Li, B. R. Cemlyn, H. Susanto, and I. D. Henning, Phys. Rev. A **95**, 053869 (2017).

[43] R. D. Li and T. Erneux, Phys. Rev. A **46**, 4252 (1992).

[44] H. Dave, Z. Gao, and K. D. Choquette, Appl. Phys. Lett. **117**, 041106 (2020).

[45] N. Hatano and D. R. Nelson, Phys. Rev. Lett. **77**, 570 (1996).

[46] Z. Shao, J. Zhu, Y. Chen, Y. Zhang, and S. Yu, Nat. Commun. **9**, 926 (2018).

[47] T. Chen, H. Lee, J. Li, and K. J. Vahala, Opt. Express **20**, 22819 (2012).

[48] Y. Yu, M. Jung, and G. Shvets, Phys. Rev. B **103**, L041102 (2021).

[49] J. D. H. Rivero and L. Ge, Phys. Rev. B **103**, 014111 (2021).

[50] K. Kawabata, M. Sato, and K. Shiozaki, Phys. Rev. B **102**, 205118 (2020).

[51] M. M. Denner, A. Skurativska, F. Schindler, M. H. Fischer, R. Thomale, T. Bzdušek, and T. Neupert, Nat. Commun. **12**, 5681 (2021).

[52] K. Kawabata, K. Shiozaki, and S. Ryu, Phys. Rev. Lett. **126**, 216405 (2021).

[53] L. Ge, Phys. Rev. A **95**, 023812 (2017).

[54] H. Dave, P. Liao, S. T. M. Fryslie, Z. Gao, B. J. Thompson, A. E. Willner, and K. D. Choquette, IEEE Photonics Technol. Lett. **31**, 173 (2019).

[55] Y. Kominis, A. Bountis, and V. Kovanis, J. Appl. Phys. **127**, 083103 (2020).

[56] K. Takata, S. Utsunomiya, and Y. Yamamoto, New J. Phys. **14**, 013052 (2012).

[57] J. Robertson, M. Hejda, J. Bueno, and A. Hurtado, Sci. Rep. **10**, 6098 (2020).